Drug Design, Development and Therapy

Dovepress
Taylor & Francis Group

Open Access Full Text Article

ORIGINAL RESEARCH

Integrating Network Pharmacology and Experimental Validation to Investigate the Action Mechanism of Allicin in Atherosclerosis

Shuaikai Wu[1], Tingting Liu[1], Mingjin Weng[2], Yuping Zhou[3], Lijing Ye[1], Suyan Ruan[3], Dongmei Tang[4], Qiong Zhong[1], Lili Liu[1], Guojun Zhao[1]

[1]The Afiliated Qingyuan Hospital (Qingyuan People's Hospital), Guangzhou Medical University, Qingyuan, Guangdong, People's Republic of China; [2]School of Pharmacy, Zunyi Medical University, Zhuhai, Guangdong, People's Republic of China; [3]College of Basic Medical Sciences, Dali University, Dali, Yunnan, People's Republic of China; [4]School of Artificial Intelligence Medicicine, Guilin Medical University, Guilin, Guangxi, People's Republic of China

Correspondence: Guojun Zhao, The Afiliated Qingyuan Hospital (Qingyuan People's Hospital), Guangzhou Medical University, No. 35, Yinquan North Road, Qingcheng District, Qingyuan, Guangdong, 511518, People's Republic of China, Tel +86-18820540486, Email zhaoguojun@gzhmu.edu.cn

Background: Allicin is a monomer compound derived from traditional Chinese medicine, which has demonstrated significant efficacy in the treatment of cancer, neuroinflammation, gastrointestinal diseases, and other conditions. However, the specific mechanism of action of Allicin in combating cardiovascular diseases remains insufficiently clarified, which limits its application in therapy.

Methods: Network pharmacology and molecular docking techniques were employed to explore the potential targets and signaling pathways of Allicin in the treatment of as atherosclerosis (AS). The regulatory effects of Allicin on cell apoptosis, aortic plaques, and lipid levels were assessed through TUNEL staining, Oil Red O staining, HE staining, GPO-PAP, and COD-PAP. Additionally, immunofluorescence assay was conducted to validate the screened key targets.

Results: Based on the analysis of network pharmacology and molecular docking techniques, 94 predicted overlapping target genes were identified from the target genes of Allicin and AS-related target genes; Among them, Allicin exhibits a strong binding affinity for five main targets (CASP3, NF-κB1, BTK, MAPK3, and PARP1), and these targets were found to play important role in the anti-apoptotic mechanism of Allicin. Furthermore, Allicin could inhibit the progression of plaques, down- regulating the expressions of CASP3 and NF-κB1, and up-regulate the expressions of BTK, MAPK3, and PARP1 in vivo and in vitro.

Conclusion: The present results show that Allicin may improves AS by regulating the main targets of macrophage apoptosis.

Keywords: allicin, atherosclerosis, apoptosis, network pharmacology, molecular docking techniques, experimental verification

Introduction

Atherosclerosis (AS) and its secondary plaque rupture with acute cardiovascular events have always been a major contributor to morbidity and mortality worldwide.[1,2] As a systemic vascular disease with disorders of lipid metabolism as the primary factor and persistent vascular inflammation as the core of the pathology, the early stage of the disease is characterized by an inflammatory microenvironment that stimulates the transformation of macrophages into lipid droplet-rich foam cells. As the disease progresses, macrophage apoptosis triggers the release of intracellular lipids, which significantly contributes to the formation of the necrotic core of the plaque. Notably, plaques composed of cholesterol crystals, calcium salts, and other substances released by apoptotic macrophages continue to be deposited in the vessel wall, accelerating the process of arterial lumen narrowing and vascular sclerosis.[3] Despite the significant progress in the treatment of AS, there are still bottlenecks in drug therapy, such as efficacy limitations and adverse drug reactions, and a breakthrough is urgently needed through novel therapeutic strategies targeting the pathologic mechanisms.[4]

The unique therapeutic advantages of natural medicines in the field of modern disease prevention and treatment are attributable to their multi-target and multi-pathway synergistic regulation characteristics.[5,6] Natural medicines have

Received: 2 August 2025
Accepted: 6 December 2025
Published: 16 December 2025

Graphical Abstract

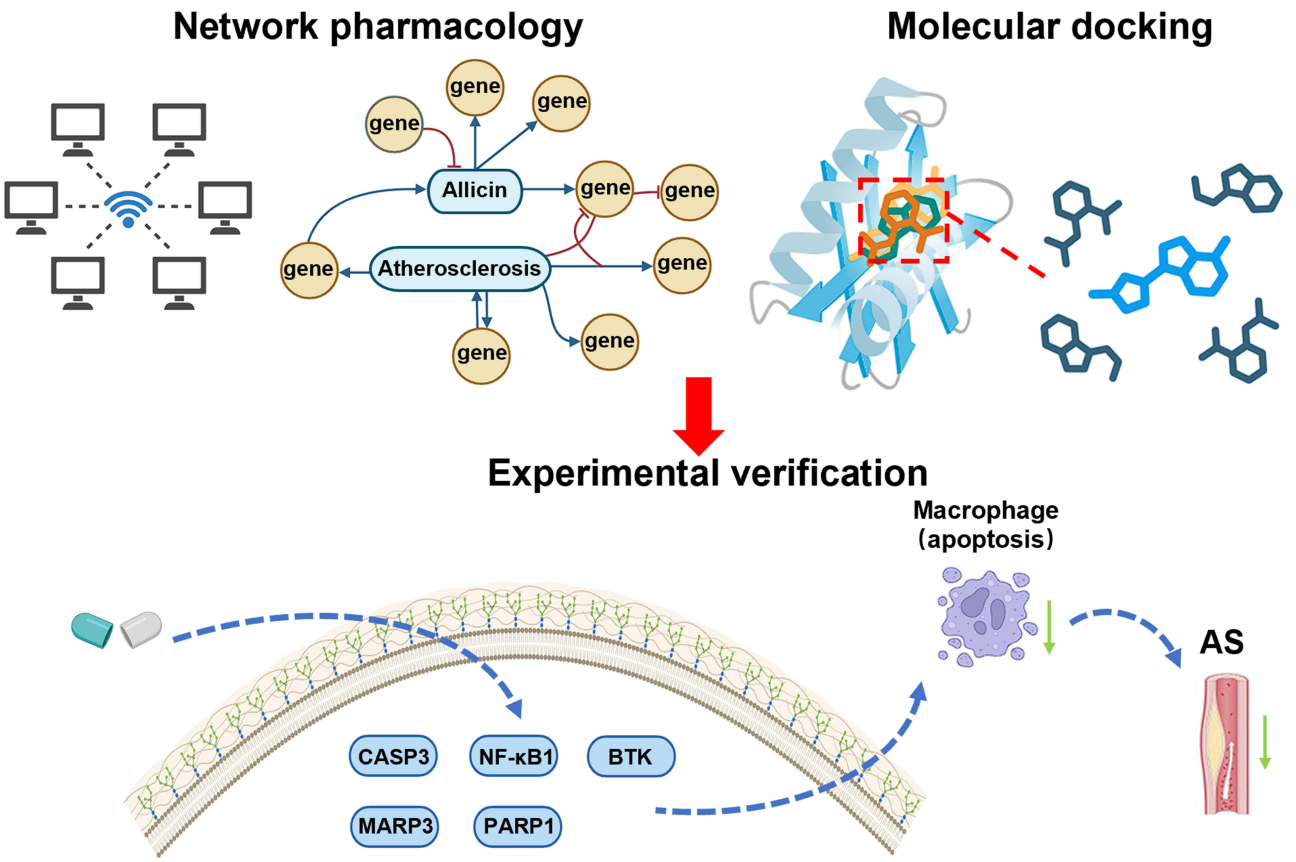

special benefits for preventing and treating modern diseases. In recent years, we have made big progress in how we analyse natural medicines. This means we can get more active ingredients out of them and purify them more easily.[7] Allicin is an organosulfur compound extracted from the bulb of garlic, a plant in the genus Allium, family Allium. As a major naturally active ingredient, it has a great cardioprotective effect on the heart and mediates various pathological processes associated with cardiovascular disease, including secretion of inflammatory factors, apoptosis of cardiomyocytes and oxidative stress. At the same time, it protects the vascular endothelial function by activating the antioxidant pathway to eliminate oxygen free radicals and reduces the production of lipid peroxidation end-products, thereby blocking the pathologic process of plaque formation.[8]

Network Pharmacology is an advanced interdisciplinary field that integrates systems biology, network biology and computational science.[9] It systematically analyses the intervention mechanism of drugs on complex disease networks by constructing a multi-dimensional interaction network of "compound-target-pathway-disease". Through the utilisation of molecular docking and other three-dimensional structure simulation techniques, the specific binding modes between small molecules and target proteins are elucidated at the atomic level.[10,11] Furthermore, the molecular mechanisms of the signalling pathways synergistically regulated by multiple components of traditional Chinese medicines are revealed through the dual-track strategy of computational prediction and experimental validation.[12–15] This approach was utilised to investigate the mechanism of the anti-atherosclerotic effect of Allicin and its predicted targets, with a view to obtaining a clearer therapeutic mechanism.

Materials and Methods

Potential Targets Identification of Allicin and AS

Materials and reagents based on a systems pharmacology strategy, the potential Allicin targets were jointly predicted using the TCMSP (https://tcmsp-e.com/) database and analysis platform, Super-PRED (https://prediction.charite.de/), and the Swiss Target Prediction (https://www.swisstargetprediction.ch/) web tool. Concurrently, the GeneCards (https://www.genecards.org/) database and the DisGeNET (https://www.disgenet.org/) database were used to identify disease targets associated with AS. After integrating the data and removing duplicate targets using the R language (version 4.2.1), the intersection between Allicin targets and disease targets was taken to generate an interactive Venn diagram, thereby screening out the potential therapeutic effects of Allicin on AS.

Construction of Protein-Protein Interaction (PPI) Networks and Screening of Key Targets

A protein-protein interaction network of potential targets of Allicin and core related targets of AS was constructed by using a network pharmacology strategy, based on the STRING database. This approach resulted in five isolated nodes without interaction relationships being hidden. The topology of the network was visualized using Cytoscape 3.10.2 software, and node topological metrics were calculated using the CytoNCA plugin, including betweenness centrality (BC), closeness centrality (CC), degree centrality (DC), eigenvector centrality (EC), network centrality (NC), and local average connectivity (LAC). The closer a node is to the center of the graph and the darker its color, the stronger its influence on the AS.

Functional Enrichment Analyses

In this study, we employed a combination of the R language (version 4.2.1) and bioinformatics toolkits (including pathview, KEGGREST, clusterProfiler, DOSE) to conduct Gene Ontology (GO) and Kyoto Encyclopedia of Genes and Genomes (KEGG) functional analysis on the core targets, with the screening threshold set at a $Q < 0.05$. The top 30 KEGG pathways ranked by significance (ascending by p value) were functionally annotated using the DAVID database (https://david.ncifcrf.gov/). The ensuing results were then represented in a bubble diagram. Furthermore, KEGG-predicted apoptotic signalling pathways were mapped using R software. With key nodes highlighted in red to represent the potential molecular mechanisms regulated by Allicin targets. To elucidate the target-pathway interactions, the intersection targets and the top 30 KEGG pathway data were imported into Cytoscape 3.10.2 software to construct a "drug–target–pathway–disease network". The present paper methodically uncovers the prospective therapeutic targets of Allicin in the context of AS, along with their associated signaling pathways.

Molecular Docking of Core Targets

The three-dimensional crystallographic structures of the core target proteins (CASP3, NF-κB1, BTK, MAPK3, and PARP1) were retrieved from the Protein Data Bank (PDB, https://www.rcsb.org/) with PDB IDs lqx3, 2o6l, 3gen, a-fold, and 2rd6, respectively. The receptor files were processed in AutoDockTools 1.5.7 for dehydration, hydrogenation, and charge optimization, and then saved in PDBQT format. The molecular fragment of Allicin was extracted from the TCMSP databases (MOL2 format) and preprocessed using AutoDockTools to generate the ligand PDBQT file. Molecular docking calculations were conducted using the AutoDock Vina program with default parameter settings for binding sites and a grid box covering the active pocket region. High-affinity complexes were screened based on binding energy ($\Delta G \leq -4.5$ kcal/mol), and 2D and 3D analysis diagrams were generated using Discovery Studio, with visualization performed using PyMOL 2.5.0. The results demonstrated that the absolute values of docking scores for the targeted proteins with Allicin were ranked as follows: CASP3 (−5.21 kcal/mol) > NF-κB1 (−5.12 kcal/mol) > BTK (−5.01 kcal/mol) > MAPK3 (−4.92 kcal/mol) > PARP1 (−4.76 kcal/mol), all significantly below the threshold of −4.5 kcal/mol, indicating strong binding activity and stability between the tested receptors and ligands. The results of the study demonstrated that Allcin exhibited robust binding affinity and stability towards the core targets predicted by the network pharmacology.

Materials and Reagents

Allicin (CAS: 539–86-6, purity ≥ 98%) and rosuvastatin (CAS: 147098–20-2, purity ≥ 98%) were both purchased from Shanghai Yuanye Biotechnology Co, Ltd (Shanghai, China). The detection kits for total cholesterol (T-CHO), low-density lipoprotein (LDL-C), and triglycerides (TG), as well as the staining kit, were procured from the Nanjing Jiancheng Bioengineering Institute (Nanjing, China). The caspase-3 primary antibody was purchased from Cell Signaling Technology (USA). The PARP1, BTK, and ERK1/2 primary antibodies were purchased from Affinity Biosciences (Jiangsu, China). The NF-κB p105/p50 primary antibody was purchased from Biodragon (Suzhou, China). Haoyuan Biotech Co, Ltd (Shanghai, China) provided the secondary antibodies. All other reagents used in the experiments were of the highest-quality commercial grade and met analytical standards.

Isolation of Primary Bone Marrow-Derived Macrophages (BMDMs) From Mice

Referring to Method, to obtain BMDMs, male mice of the wild-type strain were subjected to cervical dislocation, followed by the amputation of the hind legs.[16] The femur and tibia were then trimmed of excess muscle, and the ends of the bones were cut to expose the marrow cavity. A 1 mL syringe was used to aspirate ice-cold PBS containing 1% penicillin/streptomycin to flush the marrow from one end of the marrow cavity. Filter the cell suspension through a 70 μm filter membrane (Falcon, USA) and centrifuge at 500 × g for 5 minutes. Subsequently, the supernatant PBS was aspirated, and RPMI-1640 medium (containing 10% heat-inactivated FBS, 15% L929 cell supernatant, and 1% penicillin-streptomycin) was added. The cells underwent seeding in culture vessels (Corning, USA) and were subsequently maintained at 37°C in an atmosphere containing 5% CO_2. In addition, after 3 days of culture, an equal amount of medium was supplemented to the cells, and the culture was continued for another 2 days before the experiments were performed.

Cytotoxicity of Allicin on BMDMs

BMDMs that were in the exponential growth stage were inoculated into 96-well microplates at a cell density of 5×10^4 cells. Then, 100 μL of 1640 culture medium containing double antibody was added to every well. The cells were cultivated under conditions of 5% CO_2, 37°C, and moisture for a period of 3 days. Subsequently, 100 μL of 1640 culture media comprising double antibodies was introduced into each well, and the cells were maintained in an adherent state for an additional 48 h. After removing the old cell culture medium, the medium containing different concentrations of Allicin (0 μM, 12.5 μM, 25 μM, 50 μM, 100 μM, 200 μM) was added for coincubation for 24 h. After incubation, CCK8 (Bayotime, Jiangsu) was added and incubated in the incubator for 2 h. Finally, the optical density (OD) was measured at 450 nm using a microplate reader.

Assessment of Cell Apoptosis

The process of apoptosis was identified through the utilization of the MSCs-Tunel assay kit. BMDM cells (1×10^6 cells) were cultured in a 6-well plate and treated for 24 h with Allicin (25 μM, 50 μM). After 4 h of stimulation with etoposide (10 ng/mL) at 37°C, the medium was removed, and the cells were incubated in 4% paraformaldehyde for 10 minutes at ambient temperature.[17] Thereafter, the cells were washed three consecutive times with PBS. The working medium from the Tunel kit was meticulously dispensed into the wells, and the cells were then subjected to an incubation period at 37°C in a dark environment for a duration of 60 minutes. Thereafter, the cells were washed thrice with PBS. The cell nuclei were stained with DAPI. The observation of fluorescence was conducted through the utilization of a Nikon Eclipse Ti-S microscope.

Immunofluorescence

Firstly, BMDMs were seeded in 12-well cell culture plates at a density of 5×10^5 cells per well, and after the cells adhered to the wall, the cells were incubated with 4% paraformaldehyde for 10 min at room temperature. This was followed by three washes with PBS. Secondly, after washing three times with PBS, the cells were treated with 0.5% Triton X-100 for 10 min at room temperature. Next, 10% FBS was blocked for 1 h. Cells were incubated with antibodies to CASP3,

PARP1, BTK, MAPK3, and NF-κB1 for 16 h at 4°C. Finally, cell nuclei were stained with DAPI. Fluorescence analysis was performed using a Nikon Eclipse Ti-S microscope.

Animals, Ethical Approval, and Drug Administration

The present study received formal endorsement from the Ethics Committee of the Affiliated Qingyuan Hospital (Qingyuan People's Hospital), Guangzhou Medical University. (Approval No. LAEC-2024-039). The experiment was conducted in strict accordance with the guidelines for the care and utilization of animals in research settings. SPF grade male ApoE$^{-/-}$ mice, aged 6–8 weeks (weight 18–22 g), were purchased from Hangzhou Ziyuan Technology Laboratory Animal Co, Ltd, and housed in the SPF barrier environment of the Experimental Animal Center of Qingyuan People's Hospital. The mice were maintained in individually ventilated cages with free food and water access, a temperature ranging from 20.0 to 25.0°C, humidity between 40% and 70%, and a 12-hour illumination/darkness cycle. Regular disinfection was performed, and sterilized food and water were provided. After 7 days of adaptive feeding. The total sample size of the experiment was 30 mice, which were randomly divided into five groups (n = 6/group): the model group (HFD, high-fat diet-induced AS), the control group (NC, normal diet), the positive drug control group (RSV + HFD, high-fat diet + 10 mg/kg/day rosuvastatin gavage), the low-concentration Allicin group (LAL, high-fat diet + 25 mg/kg/day Allicin gavage), and the high-concentration Allicin group (HAL, high-fat diet + 100 mg/kg/day Allicin gavage). The high-fat diet (60% energy from fat) was purchased from Jiangsu Synergetic Medical Bioengineering Co, Ltd (Jiangsu, China). The intervention started at week 2, and at the end of week 10, mice were anaesthetised with isoflurane, blood was collected through the eyeballs, plasma was separated, and lipid indices (T-CHO, LDL, TG) were tested. Hearts and whole aortas were carefully dissected and fixed in 4% paraformaldehyde for pathological analysis (H&E, Oil Red O staining). The NC group was administered 1% DMSO phosphate buffer via gavage, with all other conditions consistent with the model group.

Assessment of Atherosclerotic Lesions

The heart and entire aorta were gently removed under a stereomicroscope and were fixed in 4% paraformaldehyde for 24 h. Place the tissue in a 30% sucrose solution to dehydrate, then embed it in OCT adhesive. The thoracic aorta is incised lengthwise and stained with 0.3% Oil Red O solution (Solarbio, Beijing) for 30 minutes, then decolorized in 60% isopropanol for 5 minutes. Following a period of differentiation, the fatty plaques in the lumen appeared orange or bright red, while other parts remained almost colorless. At this point, the differentiation process was terminated by washing with distilled water. After the areas of lesion of these plaques were photographed with an Olympus microscope, they were evaluated and analyzed. For atherosclerotic changes in the aortic root, continuous frozen sections of 3 or 6 μm thickness were obtained from the three aortic valves using a cryostat, and the samples from the cryosections were placed on slides. Stained with Oil Red O and Hematoxylin Eosin (H&E).

Determination of Lipid Levels in Mice

Serum TG, T-CHO, and LDL-C levels were quantified using enzyme-based kits. The detection methods were all performed according to the instructions.

Study on Differential Protein Expression in the Aortic Root

The analysis of arterial tissue protein expression was performed using the immunofluorescence technique to detect protein expression in aortic root sections. The immunofluorescence analysis procedure was performed according to the method documented in the existing research.[18]

Statistical Analysis

Experimental data are expressed as mean ± standard error of the mean (SEM), computed from three replicates. After confirming normality with the Shapiro–Wilk test, a one-way ANOVA was performed, with subsequent Bonferroni multiple comparison testing to identify differences among groups (GraphPad Prism 10.1.2 software). In the context of quantitative analysis, the p value < 0.05 was considered significant. The specific test parameters are delineated in the figure legends.

Results

Acquisition of Targets Associated with Allicin Intervention in AS

Firstly, 102 Allicin targets were obtained from the Swisstarget Prediction database ($p < 0.05$), and 123 Allicin targets were obtained from the Super-PRED database ($p < 0.05$). Following the elimination of redundant targets across the two databases, a total of 144 targets were retained for further analysis. A total of 5267 AS targets were identified from the GeneCards database ($p < 0.05$) and 2045 AS targets were identified from the disgenet database. After removing the overlapping targets between the two databases, a total of 5267 targets were retained. By intersecting the disease targets with the drug targets, 94 potential therapeutic targets of Allicin for AS were identified (Figure 1A).

Analyze and Construct the PPI Network Analysis Diagram

In the present study, a total of 94 common targets were identified in the course of an investigation into AS targets and Allicin active ingredients. In order to study the interactions among these targets, a protein-protein interaction (PPI) network composed of these overlapping targets was constructed using the STRING database. In the network construction stage, the biological species selected was Homo sapiens, with the network being constructed using the interaction gene search tool of the STRING database. The confidence threshold for the build was greater than 0.4, and it was found that there were five disconnected nodes. The PPI network contained 94 nodes (representing proteins) and 403 edges (representing protein-protein interactions)

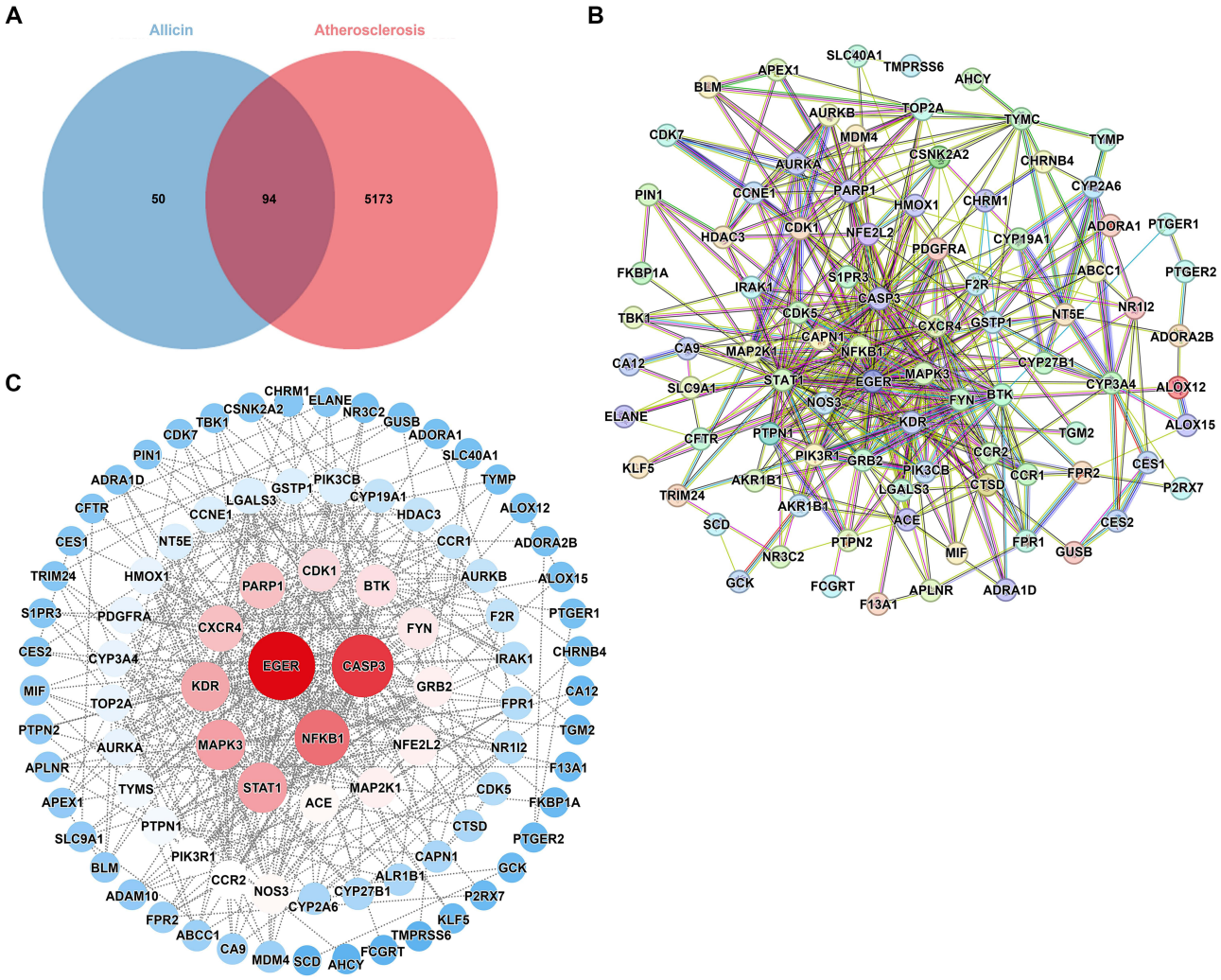

Figure 1 Identification targets of Allicin- AS. (**A**) The comment targets of Allicin and AS were shown by Venn diagram. (**B**) PPI network from STRING database imported to Cytoscape 3.10.2. (**C**) The red circle nodes represent core targets and the blue circle nodes represent noncore targets.

(Figure 1B). Subsequently, the constructed PPI network was imported into Cytoscape 3.10.2 for the purposes of visualisation and analysis. As shown in Figure 1C, the size of the nodes in the core PPI network is proportional to their degree, with larger nodes having higher degrees. Through statistical calculations, the average degree value of the nodes in the network is 8.57. To highlight the key targets, we have statistically analyzed the top 10 nodes with the highest degree values, which are EGFR (degree value = 45.0), CASP3 (degree value = 39.0), NF-κB1 (degree value = 32.0), STAT1 (degree value = 26.0), MAPK3 (degree value = 26.0), KDR (degree value = 25.0), PARP1 (degree value = 22.0), CXCR4 (degree value = 22.0), CDK1 (degree value = 19.0), and BTK (degree value = 18.0). These targets, which exhibit a high degree of interconnectedness, may assume a pivotal function in the interplay between AS and Allicin.

GO and KEGG Pathway Analysis

To investigate the functional characteristics and pathway enrichment mechanisms of the common targets (94) between Allicin and AS, this study systematically conducted GO and KEGG pathway enrichment analyses.

The results of the GO analysis showed that a total of 368 entries reached significant levels ($p < 0.05$ and $Q < 0.05$), encompassing biological processes (232 items), cellular components (62 items), and molecular functions (74 items). The top 10 entries with the highest gene counts in each category were visualized and analyzed using R software, and bar graphs were plotted to show the results, with the length and color of the bars representing the gene counts and enrichment levels, respectively (Figure 2A). As shown in Figure 2B, the BP of potential targets mainly focuses on positive regulation

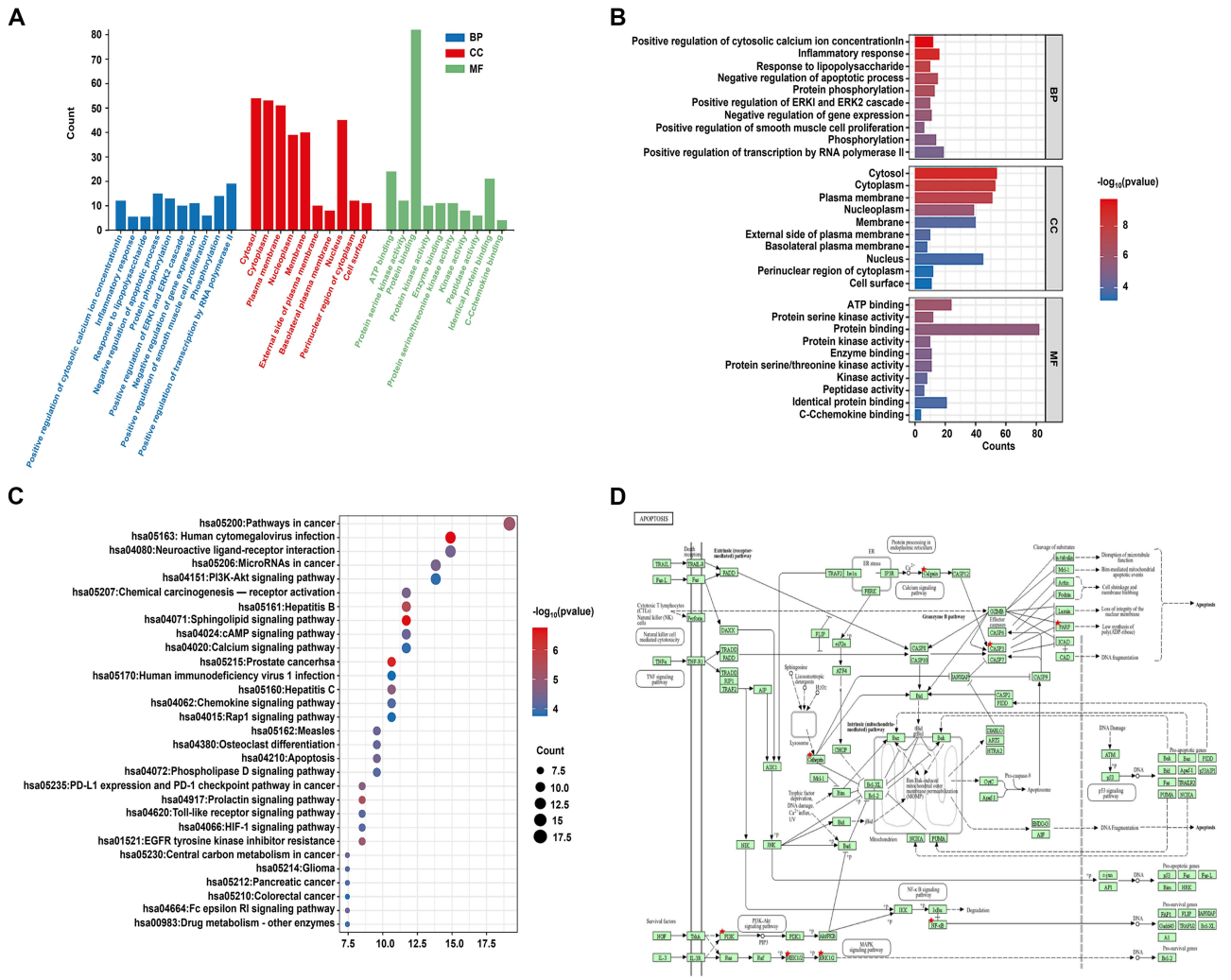

Figure 2 GO and KEGG enrichment analysis of Allicin intervening AS intersection targets. (**A** and **B**) GO enrichment analysis. (**C**) KEGG enrichment analysis. (**D**) The map of apoptosis (has04210), the red star indicates that Allicin can intervene in this pathway through these targets.

https://doi.org/10.2147/DDDT.S553875

of cytosolic calcium ion concentration (GO: 0,007,204), inflammatory response (GO: 0,006,954), response to lipopolysaccharide (GO:0,032, 496), and negative regulation of apoptotic process (GO: 0,043,066). Meanwhile, CC is enriched in Cytosol (GO: 0,005,829), Cytoplasm, Plasma membrane (GO: 0,005,737), Nucleoplasm (GO: 0,005,886), and Membrane (GO: 0,005,654). In addition, the molecular functions (MF) of potential targets are mainly concentrated in Protein binding (GO: 0,005,515), ATP binding (GO: 0,005,524), Identical protein binding (GO: 0,042,802), Protein serine kinase activity (GO: 0,004,672), Enzyme binding (GO: 0,019,899), and Protein serine threonine kinase activity (GO: 0,004,674).

Subsequently, KEGG pathway exploration was employed to identify representative pathways associated with the core targets. KEGG pathway analysis identified 122 pathways that demonstrated significant enrichment. As shown in Figure 2C, the 30 major KEGG pathways associated with Allicin are highlighted, the highly gene-enriched pathways mainly involve apoptosis (hsa04210), cancer pathways (hsa05200), PI3K-AKT pathway (hsa04151), and others. The significant enrichment of the apoptosis pathway suggests that Allicin may intervene in the progression of AS by regulating the mechanism of programmed cell death. The detailed pathway network for apoptosis and AS (hsa04210), with relevant targets marked with red stars (Figure 2D). To explore the relationships between targets and KEGG pathways, a drug- target-pathway-disease (DTPD) network consisting of 94 core targets and 30 of the most important KEGG pathways was constructed on a system using Cytoscape 3.10.2 (Figure 3). This systematic analysis has revealed the molecular mechanism of Allicin's multiple-target, multiple-pathway synergistic effects, providing a theoretical foundation for further studies of its ability to reduce AS.

Molecular Docking Analysis

In accordance with the findings of network pharmacology, the top 5 proteins were identified for further analysis: CASP3, NF-κB1, BTK, MAPK3, and PARP1. A molecular docking study was conducted using Allicin as the subject compound. The docking scores of the target proteins with Allicin were CASP3 (−5.21 kcal/mol), NF-κB1 (−5.12 kcal/mol), BTK (−5.01 kcal/mol), MAPK3 (−4.92 kcal/mol), and PARP1 (−4.76 kcal/mol) (Figure 4A). In the optimal docking mode, the absolute values of the docking scores between the target proteins and Allicin, in descending order, were CASP3, NF-κB1, BTK, MAPK3, and PARP1. Their binding energies were found to be lower than −4.5 kcal/mol, the results indicate that there is strong binding activity and stability among the tested receptors and ligands. The PyMoL 2.3.0 software was used to optimize the binding patterns between the target proteins and Allicin. The results show that Allicin can bind to the hydrophobic cavity of CASP3, stabilizing the complex structure by forming conventional hydrogen bonds with ILE262 and ALA200, pi-cation bonds with ASP169 and TYR203, and pi-alkyl bonds with TRP206 (Figure 4B). For NFKB1, Allicin forms an Attractive Charge interaction with GLU190, and maintains the binding by forming alkyl bonds with CYS159, VAL169, ILE194, LEU193, LEU176, and LEU173 (Figure 4C). In BTK, Allicin forms an attractive charge interaction with ASP539 and simultaneously forms conventional hydrogen bonds with THR474 to maintain the binding. And it forms pi-alkyl bond interactions with ILE472, LYS430, MET477, LEU528, ALA428, TYR476 and LEU408 (Figure 4D). MAPK3 maintains the binding with Allicin through pi-alkyl bonds interactions with LYS168 and ASN171, and a covalent bond with HIS164 (Figure 4E). The hydrophobic cavity of PARP1 can bind Allicin, maintaining the stability of the complex by forming conventional hydrogen bonds with THR206 and alkyl bond interactions with LYS23, ALA24 (Figure 4F). As shown in Table 1, the PDB IDs for CASP3, NF-κB1, BTK and PARP1 are lqx3, 2o6l, 3gen and 2rd6 respectively, while the structure of MAPK3 was predicted by Alphafold (https://alphafold.ebi.ac.uk/entry/L7RXH5).

Cytotoxicity of Allicin on BMDMs

The survival percentage (%) of BMDMs exhibited a significant concentration- dependent change with increasing Allicin concentration (Figure 5A). In contrast with the control group, the viability of BMDMs demonstrated a marked decline when the Allicin concentration surpassed 100 μM. The variation in question was determined to be statistically significant ($p < 0.01$). Therefore, in cell experiments, the concentration of Allicin should not exceed 100 μM. This study selected 25 μM and 50 μM as the subsequent experimental doses of Allicin to balance efficacy and cytotoxicity.

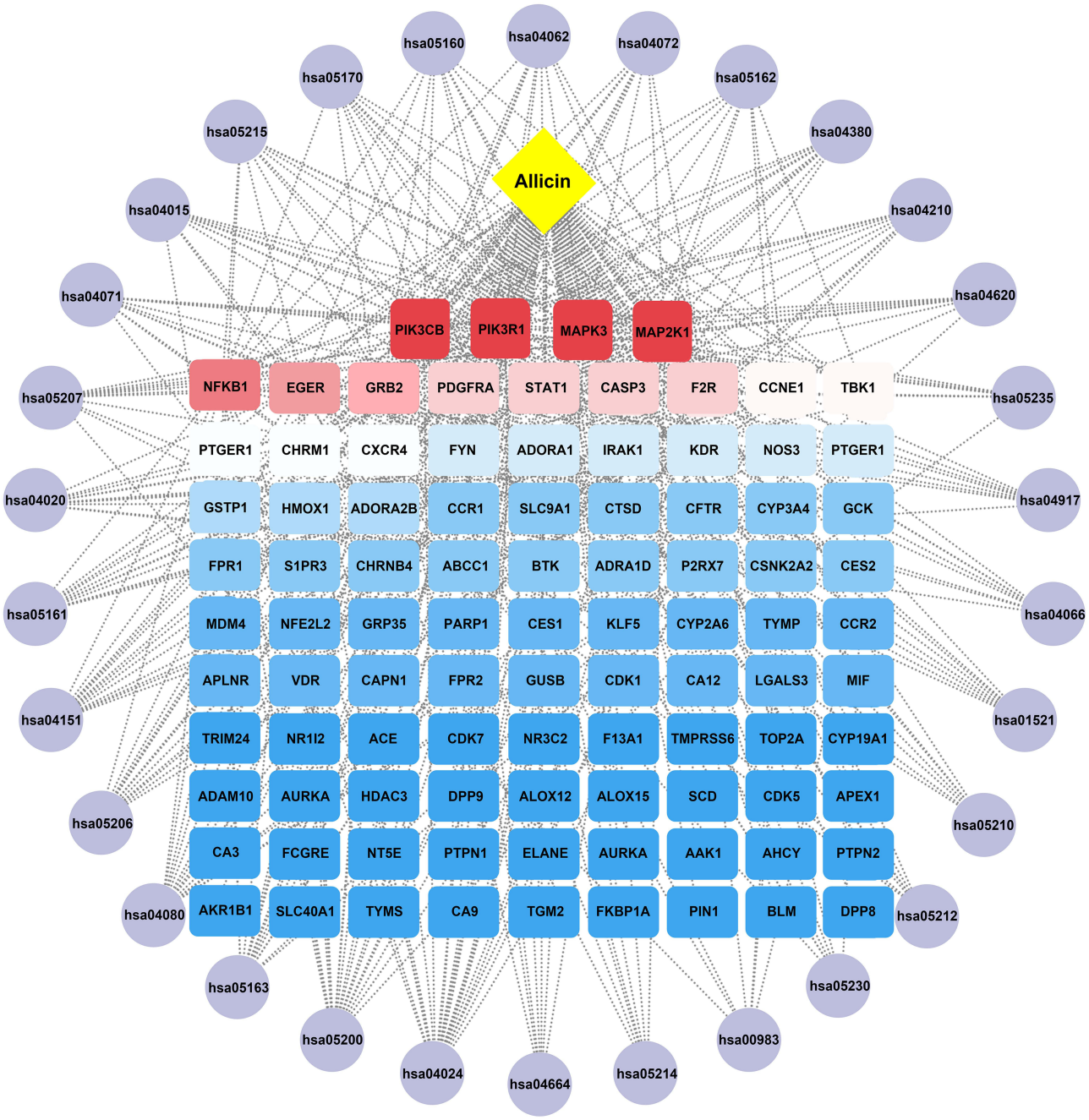

Figure 3 Drug-target-pathway-disease (DTPD) network. The potential targets of Allicin in the treatment of AS, and the interaction network associated with the therapeutic pathways.

Effects of Allicin on Etoposide Induced Apoptosis of BMDMs

In comparison with the control group, apoptosis of BMDMs was significantly induced by treatment with etoposide (10 ng/mL) for 4 h. It is noteworthy that when 25 μM and 50 μM Allicin were co-treated with etoposide, the apoptosis rate exhibited a dose-dependent decline trend (Figure 5B). In the statistical graph, the apoptosis rate of the 50 μM drug group was observed to show recovery to reach the control level (Figure 5C). These results suggest that Allicin can counteract the pro-apoptotic effect of etoposide, exhibiting a dose-dependent response.

https://doi.org/10.2147/DDDT.S553875

A

Target	Compound	Free Binding Energy (Kcal/mol)
CASP3	Allicin	-5.21
NFKB1		-5.12
BTK		-5.01
MAPK3		-4.92
PARP1		-4.76

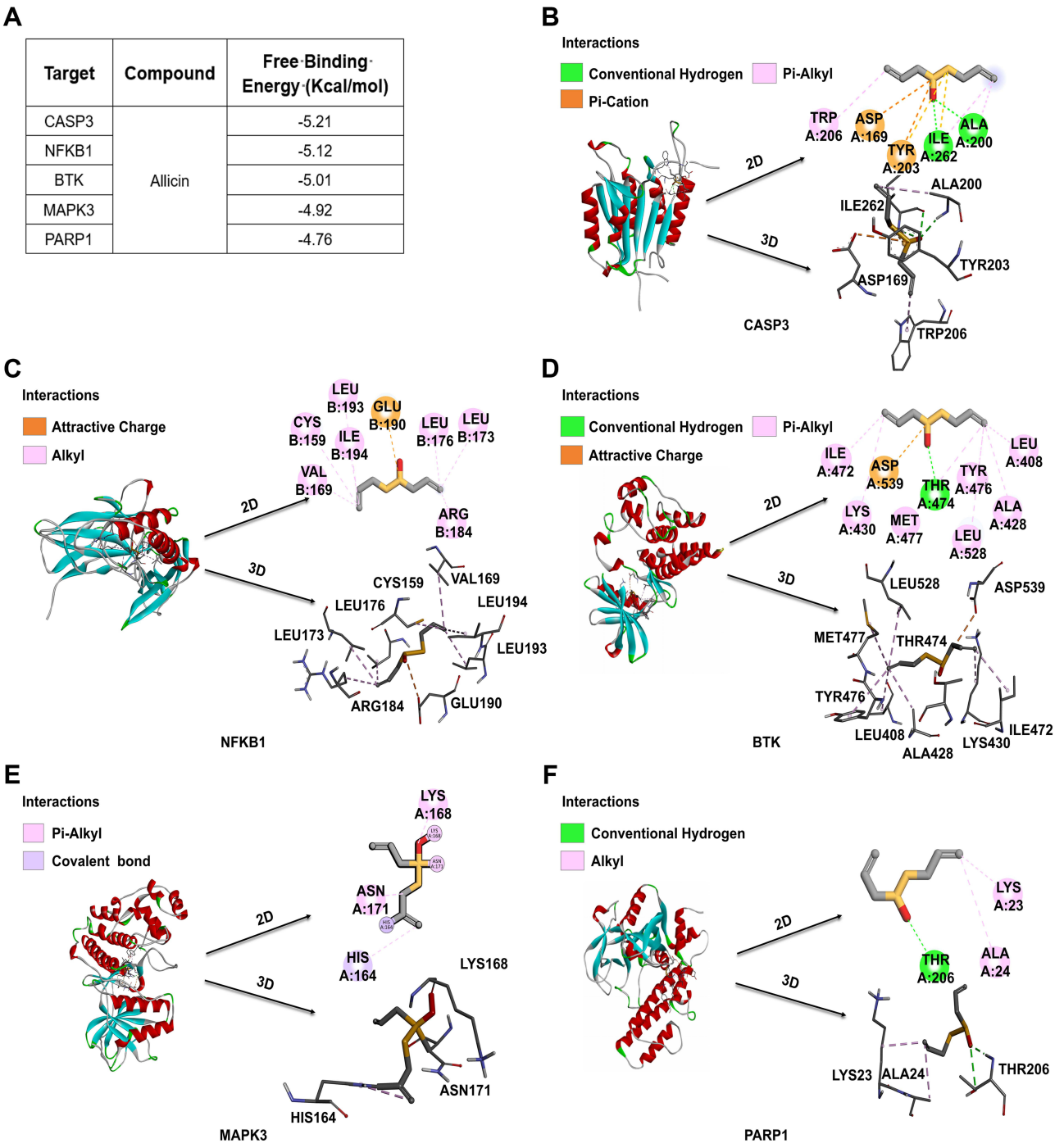

Figure 4 2D and 3D docking patterns of Molecular docking between Allicin and core targets protein. (**A**) The binding energy of molecular docking. (**B**) CASP3 and Allicin molecular docking visualization. (**C**) NF-κB1 and Allicin molecular docking visualization. (**D**) BTK and Allicin molecular docking visualization. (**E**) MAPK3 and Allicin molecular docking visualization. (**F**) PARP1 and Allicin molecular docking visualization.

Allicin Reversed the Induction of Target Proteins in BMDMs by Etoposide

Through network pharmacology and molecular docking analysis, we predicted that the core target proteins of Allicin's anti- AS were CASP3, NF-κB1, MAPK3, PARP1, and BTK, and focused on the changes of these proteins in the disease. In comparison with the control group, Etoposide (10 ng/mL) demonstrated a significant upregulation of CASP3 and NF-κB1 in BMDMs and a significant downregulation of MAPK3, PARP1 and BTK. However, after combined intervention with Allicin, the abnormal expression of these proteins induced by Etoposide showed

Table 1 The Binding Energy of Top 5 Compound-Protein Pairings

Compound-Protein Pairings	PDB ID	Binding Energy (kJ/mol)
CASP3	1qx3	−5.21
NFKB1	2o61	−5.12
BTK	3gen	−5.01
MAPK3		−4.92
PARP1	2rd6	−4.76

Note: The structure of MAPK3 was predicted by AlphaFold.

a dose-dependent reversal trend (Figure 6A–J). The aforementioned results suggest that Allicin can modulate the expression of CASP3, NF-κB1, BTK, MAPK3, and PARP1 proteins associated with BMDMs at the cellular level.

Allicin Ameliorates Aortic Plaque Formation and Serum Lipid Disorders Induced by High-Fat Diet in ApoE$^{-/-}$ Mice

Given that AS is modeled in mice through a diet consisting of a high fat content. As shown in Figure 7A, the control group consumed a conventional diet, while the model group ingested a diet with a high fat content for a duration of 12 weeks. The positive drug group, as well as the low-dose and high-dose drug groups, initiated drug administration following a 14-day period of high-fat diet feeding, which continued for a duration of 10 weeks. The potential protective effects of Allicin on HFD-related AS in ApoE$^{-/-}$ mice were evaluated. Compared to mice on a standard diet, mice fed with HFD showed significant weight gain and fat accumulation, and Allicin treatment successfully attenuated these effects (Figure 7B and C). A systematic evaluation of the progression of the disease can be achieved by analyzing the values of total cholesterol, triglycerides, and low-density lipoprotein cholesterol in the serum of mice (Figure 7D–F). Subsequently, to evaluate the effect of Allicin on plaque formation, we performed oil red O staining of the entire aorta (Figure 8A), and quantified and statistically analyzed the area of aortic plaques. (Figure 8B). We also conducted Oil Red O and H&E staining on the lipid-rich plaques in the aortic root and made statistical analyses (Figure 8C and D). Based on the histopathological analysis of these staining results, key morphological features such as aortic plaque, lumen stenosis, and inflammatory cell infiltration were visually assessed. The statistical chart shows that compared with mice on a normal diet, mice on a high-fat diet had larger and more extensive plaque deposits on the aortic wall and the aortic root. After intervention with Allicin and rosuvastatin, the area and size of the plaques significantly decreased.

Effect of Allicin on Predicted Target Proteins Expression From Arterial

In accordance with the principles of network pharmacology and molecular docking predictions, the potential target proteins of Allicin for the treatment of AS include CASP3, NF-κB1, BTK, MAPK3, and PARP1. In order to verify the mechanisms of action of these targets, the present study investigated the protein expression levels in atherosclerotic plaques using immunofluorescence techniques. The results demonstrated that, in comparison with the NC group, the CASP3 and NF-κB1 expression levels in the thoracic aortic arteries of mice in the HFD group were significantly increased; however, after intervention with Allicin and the positive control drug Rosuvastatin, the expression levels were found to be considerably diminished (Figure 9A–D). It is noteworthy that, in contrast to the HFD group, the expression levels of MAPK3, BTK, and PARP1 in the Allicin treatment group exhibited a dose-dependent upregulation (Figure 9E–J).

The aforementioned results indicate that Allicin inhibits the progression of AS by bidirectionally regulating the pathological abnormal expression of CASP3, NF-κB1, BTK, MAPK3, and PARP1. In vivo experimental data further confirm that the multi-target regulatory effect of Allicin is an important molecular mechanism underlying its anti-atherosclerotic properties.

https://doi.org/10.2147/DDDT.S553875

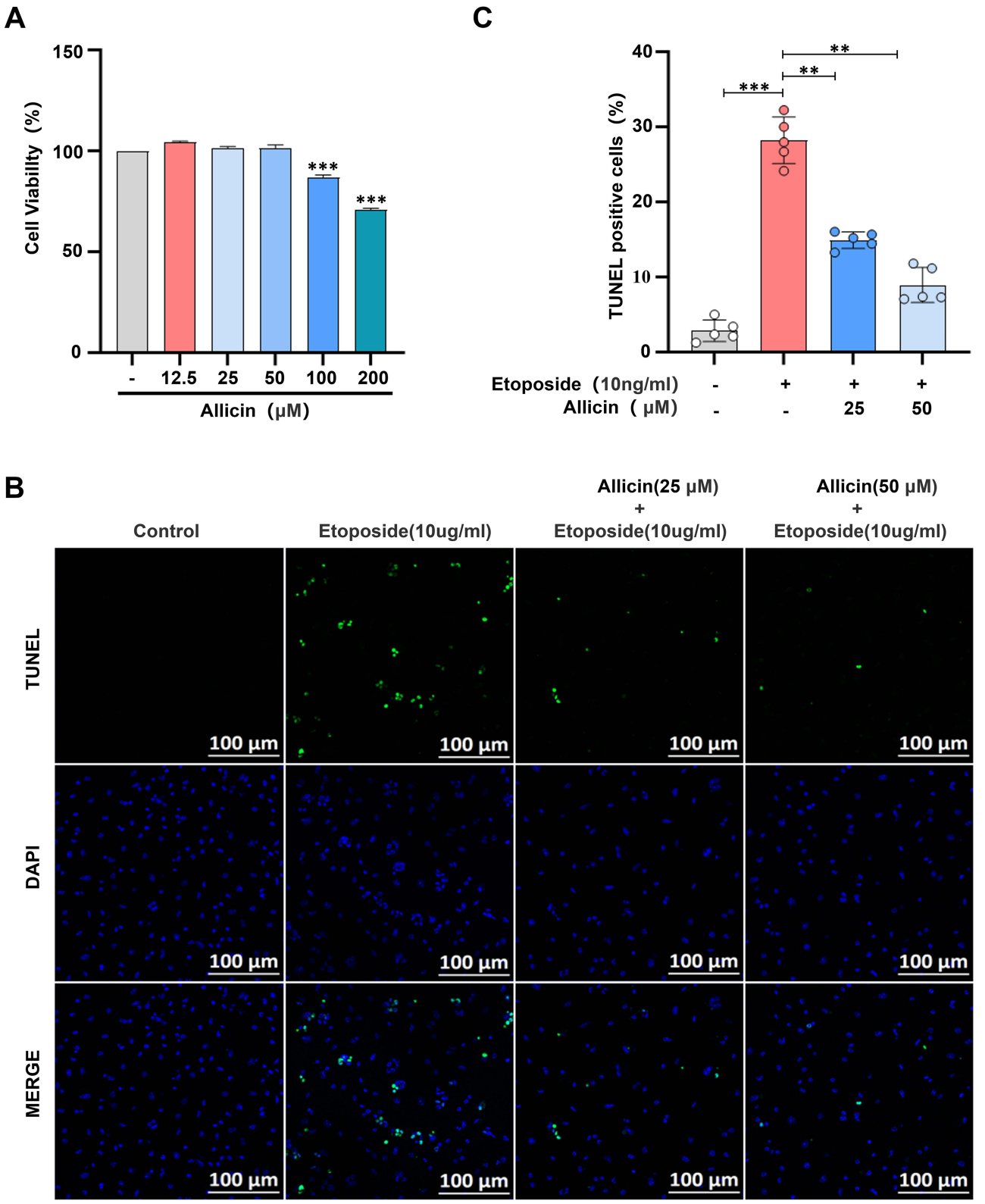

Figure 5 Effects of Allicin on Etoposide induced apoptosis of BMDMs. (**A**) Effect of Allicin on the survival rate (%) of BMDMs. (**B**) Representative images of Tunel staining, scale bar = 100 μm. (**C**) Fluorescence statistical analysis diagrams of apoptotic cells obtained through TUNEL staining. The results are presented as the mean ± SD, n = 5. After confirming normality using the Shapiro–Wilk test, a one-way ANOVA analysis of variance was conducted through Bonferroni multiple comparison test. Compared with the model group, **p < 0.01, ***p < 0.001.

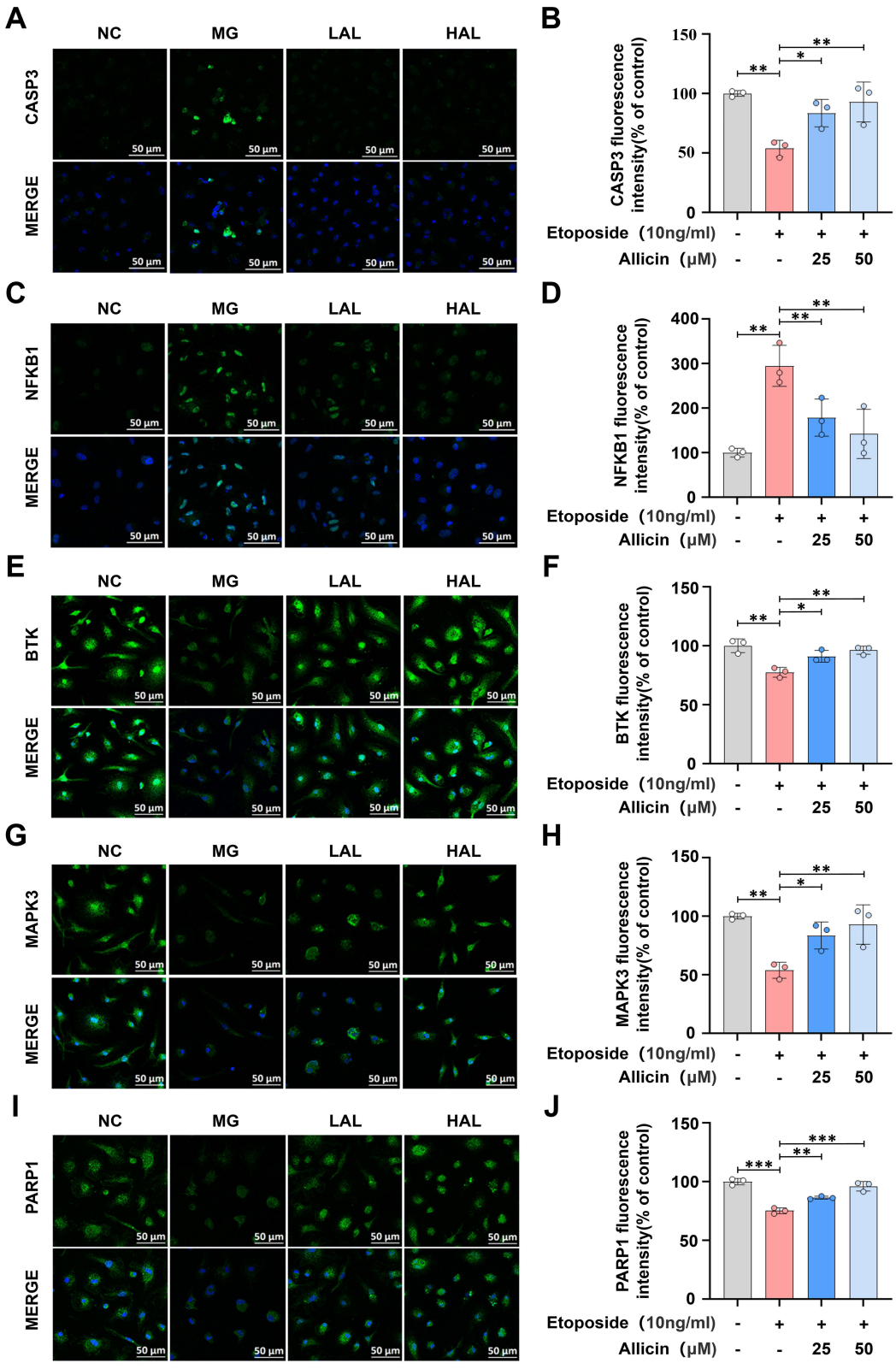

Figure 6 In vitro cellular validation of the effect of Allicin on target protein expression. (**A**) representative fluorescence picture of CASP3, scale bar = 50 μm. (**B**) Fluorescence intensity statistic analysis of CASP3. (**C**) representative fluorescence picture of NF-κB1, scale bar = 50 μm. (**D**) Fluorescence intensity statistic analysis of NF-κB1. (**E**) Representative fluorescence picture of BTK, scale bar = 50 μm. (**F**) Fluorescence intensity statistic analysis of BTK. (**G**) Representative fluorescence picture of MAPK3, scale bar = 50 μm. (**H**) Fluorescence intensity statistic analysis of MAPK3. (**I**) Representative fluorescence picture of PARP1, scale bar = 50 μm. (**J**) Fluorescence intensity statistic analysis of PARP1. The results are presented as the mean ± SD, n = 3. After confirming normality using the Shapiro–Wilk test, a one-way ANOVA analysis of variance was conducted through Bonferroni multiple comparison test. Compared with the model group, *p < 0.05, **p < 0.01, ***p < 0.001.

https://doi.org/10.2147/DDDT.S553875

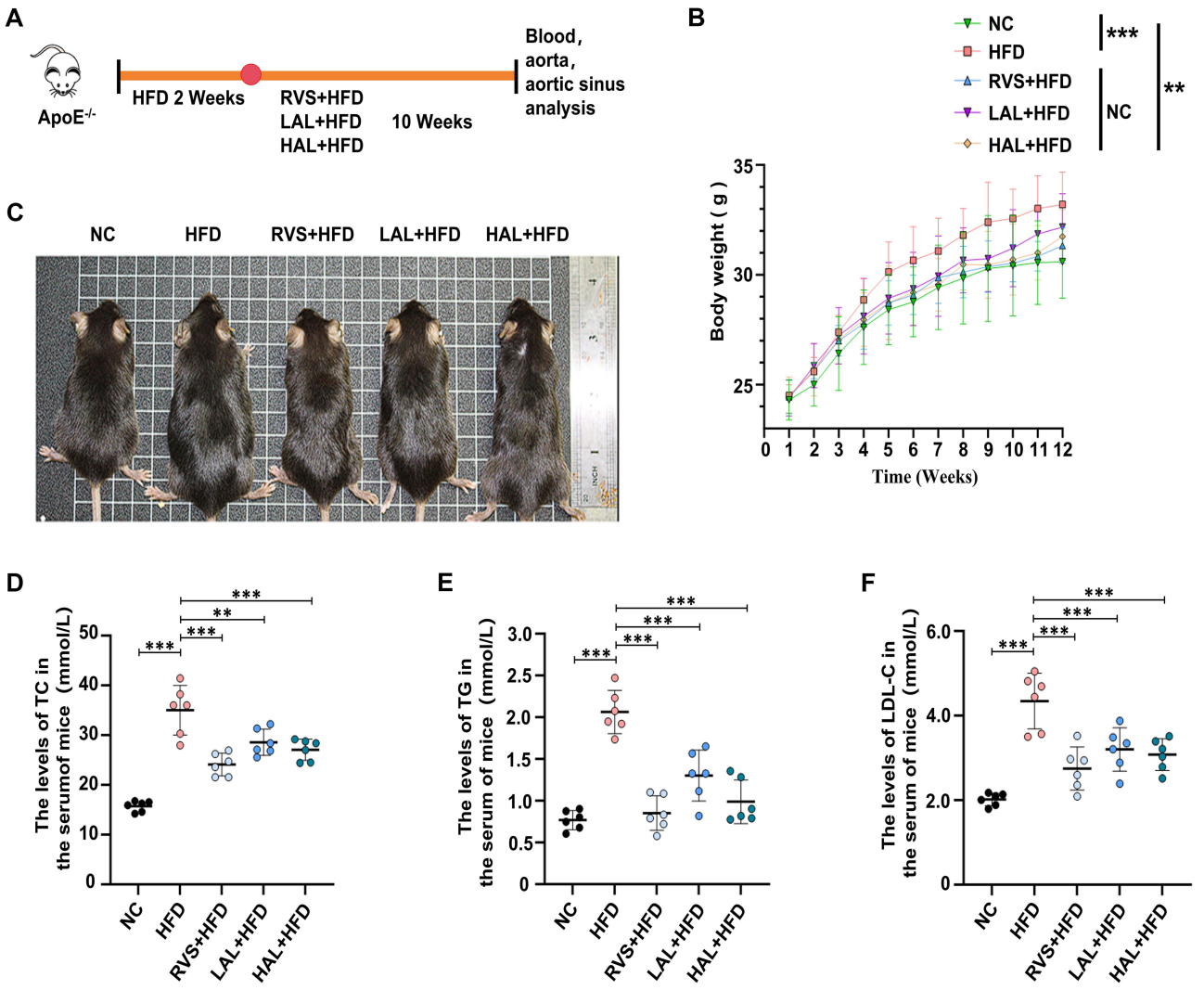

Figure 7 Allicin intervention significantly reduced body weight and blood lipid levels in the ApoE$^{-/-}$ mouse model induced by high-fat diet. (**A**) Schematic diagram of the intervention study: negative control (NC) fed normal diet, model group mice fed high-fat diet for 12 weeks, drug group fed high-fat diet for 12 weeks followed by drug intervention for 10 weeks, the mice were finally put to death. (**B**) Body weight, n = 6. (**C**) Photographs of representative mice. Lipid content measurement showed that Allicin reduced the serum levels of TC (**D**), TG (**E**) and LDL-C (**F**) in AS mice, n = 6. The results are represented as mean ± SD of 6 mice in each group. After confirming normality using the Shapiro–Wilk test, a one-way ANOVA analysis of variance was conducted through Bonferroni multiple comparison test. Compared with the model group, **p < 0.01, ***p < 0.001.

Clustering Study on the Multi-Target Regulatory Mechanisms of Allicin in Anti-AS

To systematically evaluate the anti-atherosclerotic effects of Allicin, this study normalized the efficacy indicators (plaque area) and core protein expression data (CASP3, NF-κB1, BTK, MAPK3, PARP1) of each group based on the high-fat diet model group. Hierarchical clustering analysis was employed to explore the intergroup differences in intervention effects. The results indicated substantial heterogeneity in the therapeutic response and expression profiles between the different intervention groups (RVS, HAL, LAL, HFD, NC). However, after normalization, the data exhibited a clear clustering trend. Specifically, the RSV + HFD, the LAL group, the HAL group, and the NC group clustered into one category, indicating that the intervention effect of HAL was highly similar to that of NC.

Further analysis revealed that as the dose of Allicin increased from 25 mg/kg/d to 100 mg/kg/d, its pharmacodynamic indicators (such as the reduction rate of plaque area) and target protein expression (downregulation of CASP3 and NF-κB1, upregulation of BTK, MAPK3, and PARP1) exhibited dose-dependent changes, with the intervention trajectory gradually shifting from HFD towards NC. The above results indicate that Allicin has a significant dose-dependent characteristic in intervening in the pathological process of AS and related regulatory proteins, and high-dose Allicin can restore a protein expression profile close to the physiological state through synergistic effects of multiple targets.

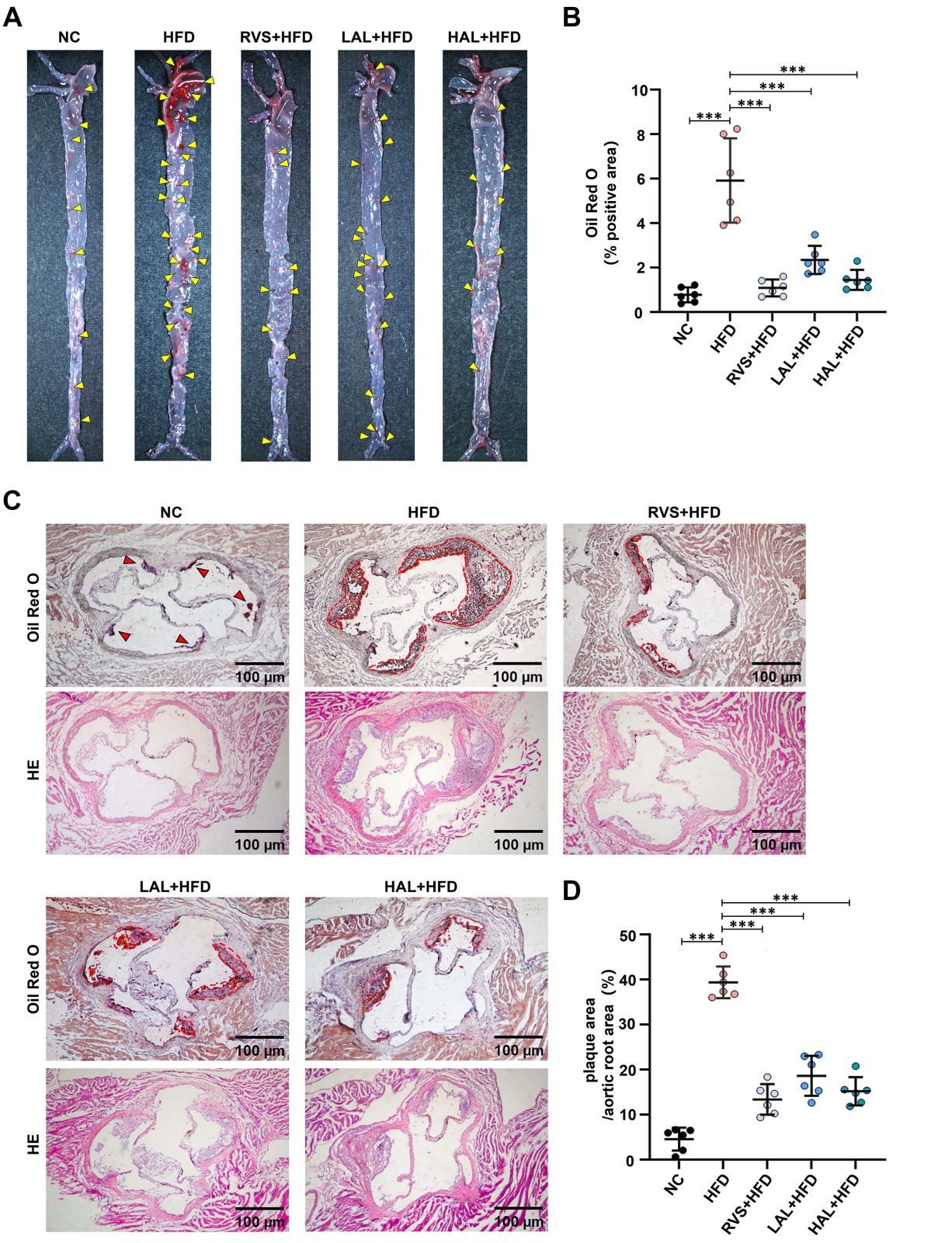

Figure 8 Allicin intervention significantly inhibits atherosclerotic plaques in the ApoE$^{-/-}$ mouse model induced by high-fat diet. (**A**) Representative images of aortas stained with Oil Red O, the yellow arrow indicates the plaque on the aorta. (**B**) Quantitative statistical analysis of plaque area in the frontal view. (**C**) Representative images of Oil Red O staining and H&E staining of the aortic root (scale bar = 100 μm), the red arrow indicates the smaller plaque at the aortic root, while the red dotted circle encloses the more severe plaque. (**D**) Quantitative statistical analysis graph of lipid content in the aortic root region by Oil Red O staining. The results are presented as the mean ± SD, n = 6. After confirming normality using the Shapiro–Wilk test, a one-way ANOVA analysis of variance was conducted through Bonferroni multiple comparison test. Compared with the model group, ***$p < 0.001$.

https://doi.org/10.2147/DDDT.S553875

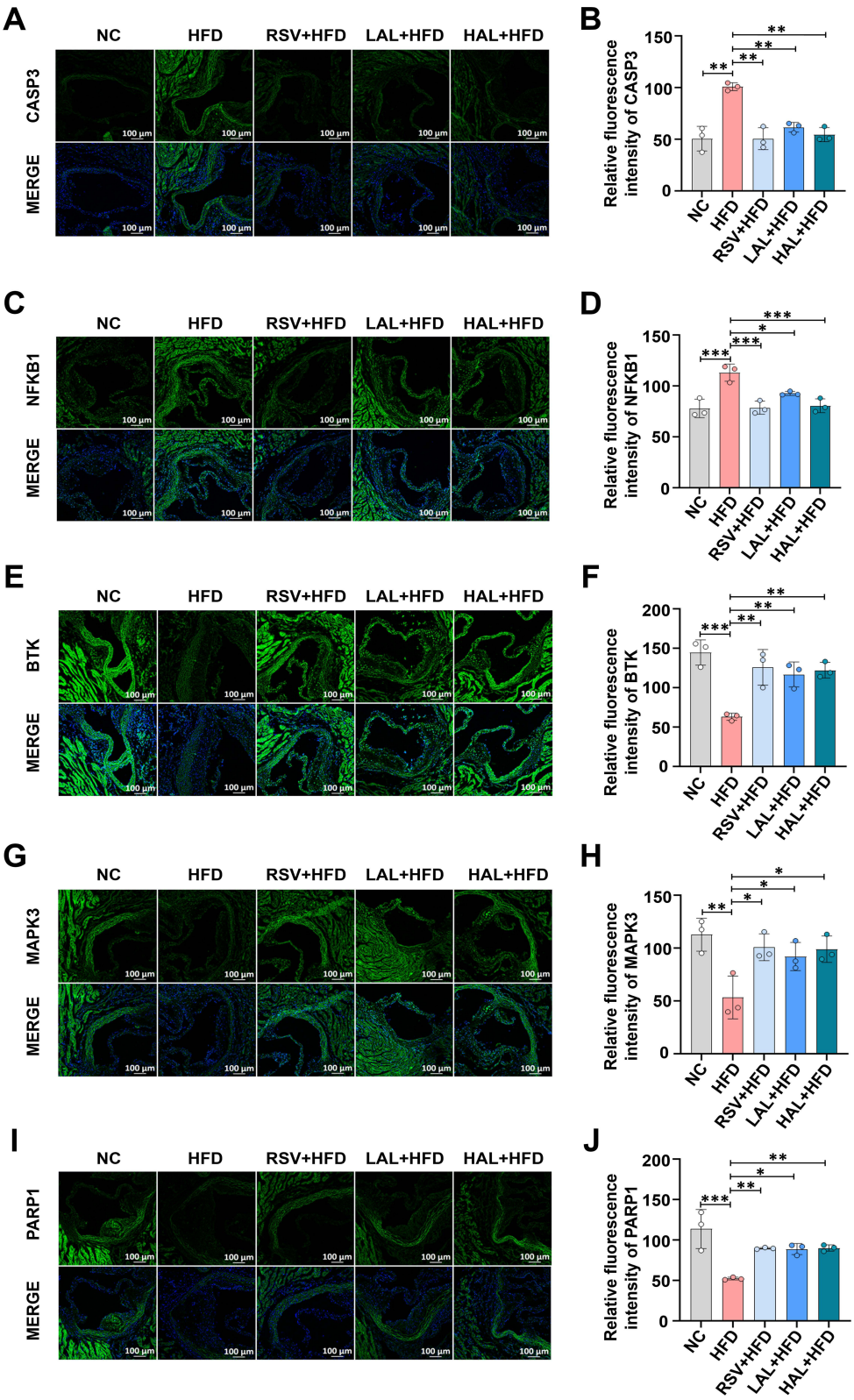

Figure 9 Verification of the expression of the predicted target proteins. (**A**) Representative fluorescence pictures of CASP3, scale bar = 100 μm. (**B**) Statistical plots of fluorescence intensity from CASP3. (**C**) Representative fluorescence pictures of NF-κB1, scale bar = 100 μm. (**D**) Statistical plots of fluorescence intensity from NF-κB1. (**E**) Representative fluorescence pictures of BTK, scale bar = 100 μm. (**F**) Statistical plots of fluorescence intensity from BTK. (**G**) Representative fluorescence pictures of MAPK3, scale bar = 100 μm. (**H**) Statistical plots of fluorescence intensity from MAPK3. (**I**) Representative fluorescence pictures of PARP1, scale bar = 100 μm. (**J**) Statistical plots of fluorescence intensity from PARP1. The results are presented as the mean ± SD, n = 3. After confirming normality using the Shapiro–Wilk test, a one-way ANOVA analysis of variance was conducted through Bonferroni multiple comparison test. *p < 0.05, **p < 0.001, ***p < 0.001.

Discussion

Previous studies have found that Allicin can inhibit the progression of AS, which has also been confirmed in our experiments.[19,20] However, its potential target genes and mechanisms of action remain unclear. Using network pharmacology, we systematically elucidated the underlying mechanisms by which Allicin suppresses AS. Furthermore, employed integrated molecular docking and experimental assays to confirm the effects of Allicin.

We identified 94 Allicin-AS related targets through the database and established a PPI network.Using bioinformatics tools, the top ten targets of Allicin against AS were determined, including EGFR, CASP3, NFKB1, STAT1, MAPK3, KDR, PARP1, CXCR4, CDK1, and BTK. Previous studies have established that these main targets play modulatory roles within the cardiovascular system, suggesting that the beneficial effects of Allicin on AS intervention can be attributed to the synergistic actions of these main targets.[21–30] GO and KEGG enrichment analyses were performed on these 94 selected targets to systematically elucidate the impact of Allicin on AS. GO analysis revealed that Allicin is primarily involved in biological processes such as the negative regulation of apoptosis, inflammatory response, and positive regulation of RNA polymerase II transcription. Meanwhile, KEGG results confirmed that the main signaling pathways through which Allicin intervenes in AS include the apoptosis pathway, pathways in cancer, and the PI3K-Akt signaling pathway. It indicates that Allicin mitigates AS progression primarily through its anti-apoptotic effect. These findings are consistent with our perspective.

Molecular docking serves as a key tool for elucidating binding mechanisms and facilitating drug molecule optimization.[31] To further investigate the binding potential of Allicin to potential AS targets, molecular docking was performed between Allicin and the top ten main targets screened via network pharmacology. The results demonstrated that Allicin exhibited favorable binding affinity with five main targets: CASP3, NF-κB1, BTK, MAPK3, and PARP1. The calculated binding energies for these complexes were all within the range of −4.76 to −5.21 kcal/mol, confirming strong binding activity. These main targets are closely associated with the apoptosis pathway, suggesting that Allicin may exert anti-apoptotic effects by modulating them.

Previous studies have shown that apoptosis of macrophages is an important link in the development of AS, which is closely associated with the dysregulation of anti-apoptotic pathways and the dysfunction of critical signaling molecules.[32,33] CASP3, identified as the target with the strongest binding affinity to Allicin, serves as the core executor of the apoptotic signaling pathway. Its activation is considered a critical marker of cells entering the apoptosis process and a key driver of aberrant macrophage apoptosis in AS.[34,35] NF-κB1 (p50/p105), a core member of the NF-κB family, participates in classical pathways including apoptosis, cell proliferation, inflammation, and immunity.[36] P50 depletion attenuates SN1-methylator-induced apoptosis, while restoration of p50 expression reinstates normal apoptotic function.[37] BTK, a non-receptor tyrosine kinase highly expressed in various immune cells such as B cells and macrophages, not only modulates inflammatory signaling but also exerts protective effects by inhibiting apoptosis.[38] BTK enhances cell survival through the suppression of apoptosis, a process mediated by the PI3K-AKT pathway. Activation of this pathway results in BAD phosphorylation, which prevents its binding to anti-apoptotic proteins BCL-2 and BCL-xL.[39] MAPK3, a key component of the MAPK (mitogen-activated protein kinase) signaling cascade, plays a pivotal role in the anti-atherosclerotic process by regulating apoptosis, survival, proliferation, and inflammatory responses.[40] MAPK3 promotes the expression of anti-apoptotic proteins and inhibits the activity of apoptosis-related factors through phosphorylation of downstream transcription factors, thereby supporting cell survival.[41] PARP1, an NAD+-dependent chromatin-associated enzyme, mediates DNA damage repair by catalyzing ADP-ribosylation. This enzyme negatively regulates apoptosis; its full-length form exerts anti-apoptotic effects via DNA repair activity, while caspase-3-mediated proteolysis cleaves it into an 89 kDa fragment, resulting in loss of DNA repair function and initiation of the apoptotic program.[42,43] We discovered that Allicin dose-dependently inhibits macrophage apoptosis. Subsequent in vivo and in vitro experiments demonstrated that Allicin treatment significantly reduced the expression of CASP3 and NF-κB1, while upregulating the expression levels of BTK, MAPK3, and PARP1. These findings suggest that Allicin may exert a protective effect on $ApoE^{-/-}$ mice by inhibiting apoptosis.

Conclusion

In conclusion, this study employed network pharmacology, molecular docking, and experimental verification methods to reveal the potential mechanism of Allicin in treating AS. Our results confirmed that Allicin can significantly improve AS by regulating key targets in the apoptotic pathway. Our findings provide stronger evidence for exploring the potential

protective mechanism of Allicin in AS, and also offer a comprehensive and innovative approach for identifying targets and potential molecular mechanisms in drug development.

Ethics Approval

This study was supported by the Ethics Committee of the Affiliated Qingyuan Hospital (Qingyuan People's Hospital), Guangzhou Medical University (Approval No. LAEC-2024-039).

Author Contributions

All authors made a significant contribution to the work reported, whether that is in the conception, study design, execution, acquisition of data, analysis and interpretation, or in all these areas; took part in drafting, revising or critically reviewing the article; gave final approval of the version to be published; have agreed on the journal to which the article has been submitted; and agree to be accountable for all aspects of the work.

Funding

This work was supported by the National Natural Science Foundation of China (81870337), the Natural Science Foundation of Guangdong Province (2024A1515012850), and the Guangdong Provincial Bureau of Traditional Chinese Medicine Research Project (20261495).

Disclosure

The authors declare that they have no known competing financial interests or personal relationships that could have appeared to influence the work reported in this paper.

References

1. Song P, Fang Z, Wang H, et al. Global and regional prevalence, burden, and risk factors for carotid atherosclerosis: a systematic review, meta-analysis, and modelling study. *Lancet Glob Health*. 2020;8(5):721–729. doi:10.1016/S2214-109X(20)30117-0
2. Adkar SS, Leeper NJ. Efferocytosis in atherosclerosis. *Nat Rev Cardiol*. 2024;21(11):762–779. doi:10.1038/s41569-024-01037-7
3. Libby P, Ridker PM, Hansson GK. Progress and challenges in translating the biology of atherosclerosis. *Nature*. 2011;473(7347):317–325. doi:10.1038/nature10146
4. Doukky R, Diemer G, Medina A, et al. Promoting appropriate use of cardiac imaging: no longer an academic exercise. *Ann Internal Med*. 2017;166(6):438–440. doi:10.7326/M16-2673
5. Atanasov AG, Zotchev SB, Dirsch VM, et al. Natural products in drug discovery: advances and opportunities. *Nat Rev Drug Discov*. 2021;20(3):200–216. doi:10.1038/s41573-020-00114-z
6. Xie S, Zhan F, Zhu J, et al. The latest advances with natural products in drug discovery and opportunities for the future: a 2025 update. *Expert Opin Drug Discov*. 2025;20(7):827–843. doi:10.1080/17460441.2025.2507382
7. Luo Z, Yin F, Wang X, et al. Progress in approved drugs from natural product resources. *Chinese J Nat Med*. 2024;22(3):195–211. doi:10.1016/S1875-5364(24)60582-0
8. Xu S, Liao Y, Qi W, et al. Current studies and potential future research directions on biological effects and related mechanisms of allicin. *Crit Rev Food Sci Nutr*. 2023;63(25):7722–7748. doi:10.1080/10408398.2022.2049691
9. Jiang M, Lu C, Zhang C, et al. Syndrome differentiation in modern research of traditional Chinese medicine. *J Ethnopharmacol*. 2012;140(3):634–642. doi:10.1016/j.jep.2012.01.033
10. Greene JA, Loscalzo J. Putting the patient back together-social medicine, network medicine, and the limits of reductionism. *N Engl J Med*. 2017;377(25):2493–2499. doi:10.1056/EJMms1706744
11. Nogales C, Mamdouh ZM, List M, et al. Network pharmacology: curing causal mechanisms instead of treating symptoms. *Trends Pharmacol Sci*. 2022;43(2):136–150. doi:10.1016/j.ips.2021.11.004
12. Tang S, Chen S, Tan X, et al. Network pharmacology prediction and molecular docking-based strategy to explore the pharmacodynamic substances and mechanism of "Mung Bean" against bacterial infection. *Drug Dev Ind Pharm*. 2022;48(2):58–68. doi:10.1080/639045.022.2094399
13. Zhao M, Feng L, Li W. Network pharmacology and experimental verification: sanQi-DanShen treats coronary heart disease by inhibiting the PI3K/AKT signaling pathway. *Drug Des Devel Ther*. 2024;18:4529–4550. doi:10.2147/DDDT.S480248
14. Dai J, Zhou X, Xu X, et al. Study on the anti-atherosclerosis mechanisms of Tanyu Tongzhi formula based on network pharmacology, Mendelian randomization, and experimental verification. *Pharm Biol*. 2024;62(1):790–802. doi:10.1080/13880209.2024.2415666
15. Liu H, Zhu L, Chen L, et al. Therapeutic potential of traditional Chinese medicine in atherosclerosis: a review. *Phytother Res*. 2022;36(11):4080–4100. doi:10.1002/ptr.7590
16. Pan X, Wan R, Wang Y, et al. Inhibition of chemically and mechanically activated Piezo1 channels as a mechanism for ameliorating atherosclerosis with salvianolic acid B. *Br J Pharmacol*. 2022;179(14):3778–3814. doi:10.1111/bph.15826
17. Van GH, Wielders SJH, Lindhout T, et al. Rolling and adhesion of apoptotic monocytes is impaired by loss of functional cell surface-expressed P-selectin glycoprotein ligand-1. *J Thromb Haemost*. 2006;4(7):1611–1617. doi:10.1111/j.1538-7836.2006.02004

18. Hamczyk MR, Nevado RM, Gonzalo P, et al. Endothelial-to-mesenchymal transition contributes to accelerated atherosclerosis in hutchinson-gilford progeria syndrome. *Circulation*. 2024;150(20):1612–1630. doi:10.1161/CIRCULATIONAHA.123.065768
19. Panyod S, Wu WK, Chen PC, et al. Atherosclerosis amelioration by allicin in raw garlic through gut microbiota and trimethylamine-N-oxide modulation. *NPJ Biofilms Microb*. 2022;8(1):4. doi:10.1038/s41522-022-00266-3
20. Liu DS, Wang SL, Li JM, et al. Allicin improves carotid artery intima-media thickness in coronary artery disease patients with hyperhomocysteinemia. *Exp Ther Med*. 2017;14(2):1722–1726. doi:10.3892/etm.2017.4698
21. Gai X, Liu F, Chen Y, et al. GOLM1 promotes atherogenesis by activating macrophage EGFR-ERK signaling cascade. *Circul Res*. 2025;136 (8):848–861. doi:10.1161/circresaha.124.325880
22. Sun J, Singh P, Österlund J, et al. Hyperglycaemia-associated caspase-3 predicts diabetes and coronary artery disease events. *J Internal Med*. 2021;290(4):855–865. doi:10.1111/joim.3327
23. Luo JY, Liu F, Zhang T, et al. Association of NFKB1 gene rs28362491 mutation with the occurrence of major adverse cardiovascular events. *BMC Cardiovascu Disord*. 2022;22(1):313. doi:10.1186/s12872-022-02755-x
24. Zhang M, Zhu Y, Zhu J, et al. circ_0086296 induced atherosclerotic lesions via the IFIT1/STAT1 feedback loop by sponging miR-576-3p. *Cell Mol Biol Lett*. 2022;27(1):80. doi:10.1186/s11658-022-00372-2
25. Valanti EK, Dalakoura KK, Fotakis P, et al. Reconstituted HDL-apoE3 promotes endothelial cell migration through ID1 and its downstream kinases ERK1/2, AKT and p38 MAPK. *Metabolism*. 2022;127:154954. doi:10.1016/j.metabol.2021.154954
26. Liang X, Liu S, Liu G, et al. LncRNA SNHG15 promotes angiogenesis and improves cardiac repair after myocardial infarction through MiR-665-mediated KDR expression. *Cell Mol Life Sci*. 2025;82(1):211. doi:10.1007/s00018-025-05737-2
27. Xu W, Wu Y, Mao R, et al. Poly(ADP-ribose) polymerase 1 orchestrates vascular smooth muscle cell homeostasis in arterial disease. *Exp Mol Med*. 2025;57(8):1686–1699.
28. Wang Q, Meng L, Xu R, et al. Relationship between CXCR4 and GNG4 in the brain and chronic stress-induced atherosclerosis. *J Mol Med*. 2025;103(9):1113–1134. doi:10.1007/0109-25-02572-7
29. Xu H, Wang X, Yu W, et al. Syntaxin 17 protects against heart failure through recruitment of CDK1 to promote DRP1-dependent mitophagy. *JACC*. 2023;8(9):215–1239. doi:10.1016/j.jacbts.2023.04.006
30. Zheng K, Yang W, Wang S, et al. Identification of immune infiltration-related biomarkers in carotid atherosclerotic plaques. *Sci Rep*. 2023;13 (1):14153. doi:10.1038/s41598-023-40530-w
31. Paggi JM, Pandit A, Dror RO. The art and science of molecular docking. *Annu Rev Biochem*. 2024;93(1):389–410. doi:10.1146/annurev-biochem -030222-120000
32. De Meyer GRY, Zurek M, Puylaert P, et al. Programmed death of macrophages in atherosclerosis: mechanisms and therapeutic targets. *Nat Rev Cardiol*. 2024;21(5):312–325. doi:10.1038/s41569-023-00957-0
33. Van KK, Demandt JAF, Perales PNJ, et al. Deficiency of myeloid PHD proteins aggravates atherogenesis via macrophage apoptosis and paracrine fibrotic signalling. *Cardiovascu Res*. 2022;118(5):1232–1246. doi:10.1093/cvr/cvab152
34. Li X, Li Y, Qiu Q, et al. Efficient biofunctionalization of MoS2 nanosheets with peptides as intracellular fluorescent biosensor for sensitive detection of caspase-3 activity. *J Colloid Interface Sci*. 2019;543:96–105. doi:10.1016/j.jcis.2019.02.011
35. Sinha SK, Miikeda A, Fouladian Z, et al. Local M-CSF (macrophage colony-stimulating factor) expression regulates macrophage proliferation and apoptosis in atherosclerosis. *Arterioscler Thrombosis Vasc Biol*. 2021;41(1):220–233. doi:10.1161/ATVBAHA.120.315255
36. Yu Y, Wan Y, Huang C. The biological functions of NF-kappaB1 (p50) and its potential as an anti-cancer target. *Curr Cancer Drug Targets*. 2009;9 (4):566–571. doi:10.2174/156800909788486759
37. Schmitt AM, Crawley C, Kang S, et al. p50 (NF-κB1) is an effector protein in the cytotoxic response to DNA methylation damage. *Molecular Cell*. 2011;44(5):785–796. doi:10.1016/j.molcel.2011.09.026
38. Uckun FM, Venkatachalam T. Targeting solid tumors with BTK inhibitors. *Front Cell Develop Biol*. 2021;9:650414. doi:10.3389/fcell.2021.650414
39. Nyhoff LE, Griffith AS, Clark ES, et al. Btk supports autoreactive B cell development and protects against apoptosis but is expendable for antigen presentation. *J Immunol*. 2021;207(12):2922–2932. doi:10.4049/jimmunol.2000558
40. Farahani M, Robati RM, Rezaei-Tavirani M, et al. Integrating protein interaction and pathway crosstalk network reveals a promising therapeutic approach for psoriasis through apoptosis induction. *Sci Rep*. 2024;14(1):22103. doi:10.1038/s41598-024-73746-5
41. Song Y, Wang K, Loor JJ, et al. β-Hydroxybutyrate inhibits apoptosis in bovine neutrophils through activating ERK1/2 and AKT signaling pathways. *J Dairy Sci*. 2022;105(4):3477–3489. doi:10.3168/jds.2021-21259
42. Ray CA, Nussenzweig A. The multifaceted roles of PARP1 in DNA repair and chromatin remodelling. *Nat Rev Mol Cell Biol*. 2017;18 (10):610–621. doi:10.1038/nrm.2017.53
43. Ghosh U, Bhattacharyya NP. Induction of apoptosis by the inhibitors of poly (ADP-ribose) polymerase in HeLa cells. *Mol Cell Biochem*. 2009;320 (1–2):15–23. doi:10.1007/s11010-008-9894-2